Full Length Research Paper

Fusion of low and high resolution satellite images to monitor changes on costal zones

O. Gungor[1][*], Y. Boz[2], E. Gokalp[1], C. Comert[1] and A. Akar[1]

[1]Department of Geomatics, Karadeniz Technical University, Trabzon, Turkey.
[2]Department of Geomatics, Hacettepe University, Ankara, Turkey.

A low resolution ETM+ and higher resolution IKONOS images obtained in 2000 - 2003, respectively, are compared using post-classification comparison algorithm to detect changes due to a new major highway construction initiated in 2000. The spatial resolution difference between the input images, which may lead to wrong registration, thereby, wrong post-classification comparison results, are minimized by fusing the 30 meter resolution ETM+ multispectral bands with its 15 meter resolution panchromatic band using à trous wavelet transform image fusion method. The IKONOS image has color change on the sea surface especially at the river mouth and its vicinity because of mud and sediments carried by Degirmendere Creek. Therefore, maximum Likelihood, Spectral Angular Mapping, Fisher Linear Likelihood, and ECHO classifiers are used for image classification. The best results are obtained from the ECHO classifier since it considers both spectral and spatial variations in the input images. The results show that the land fill on costal zone due to new high way construction is detected successfully with ECHO classifier. It is also seen that improving the spatial resolution of the ETM+ via image fusion minimizes the impact of misclassification on final change image generated by post-classification comparison.

Key words: Change detection, image fusion, à trous wavelet transform, ETM+, IKONOS, ECHO classifier.

INTRODUCTION

Change detection is the process of identifying thematic change information occurred on earth's surface at different times. Timely and accurate change detection of earth's surface is very important since it helps in understanding the relationship and interactions between human and natural phenomena to better manage and use land resources. Change detection is widely used in many applications such as detection of change in land-cover, land-use, forest, coastal zones, etc. (Ramachandra and Kumar, 2004).

Land-cover refers to the physical material at the surface of the earth including vegetation, water, soil, and physical features those created by human activities such as buildings, asphalt, etc. The land-cover changes occur naturally in a progressive and gradual way, however, some times it may be rapid and abrupt due to human

activities and interactions (Ramachandra and Kumar, 2004), and it is very important to detect the rate and dimension of these changes. The change on coastal areas is also crucial in environmental monitoring since the impact of human activities and natural processes on the coastal environment is a major concern (Huang and Fu, 2000; Chen and Rau, 1998). Coastal zones are the borders between water and land. The co-existence of human activities and natural resources often creates conflicts of use in the coastal zones, and coastal zones are subject to a constant change which often results in negative effects on their natural structure.

Maps of coastal zones are produced via ground surveys, aerial images, lidar technology, or satellite images. Although, it offers high accuracy, mapping coastal resources by ground surveys is costly, labor intensive and time consuming (Huang and Fu, 2000; Chen and Rau, 1998). Airborne imagery provides adequate information about coastal zone, yet data acquisition and data reduction process also costly and

---
*Corresponding author. E-mail: oguzgungor@gmail.com.

time consuming at a certain degree (Chen and Rau, 1998). Lidar technology has some advantages over traditional photogrammetry and land surveying for topographic mapping since it offers high accuracy, fast acquisition and processing time with minimum human dependence. However, especially airborne lidar systems are expensive and are currently less available. On the other hand, using high resolution satellite data, large coastal areas can be mapped at regular time intervals with larger ground coverage and revisit capability of remote sensing satellites. Having multispectral optical sensors is another advantage of satellite images. Thus, satellite imagery provides a good alternative for mapping and detecting coastal changes because of its general availability, large ground coverage, sufficient information contents, and the trend of higher spatial resolution (Chen and Rau, 1998).

In ideal case, the remotely sensed data are acquired by a sensor system which collects data with the same spatial resolution on each date. However, it is not always possible to have same spatial resolution image data of the scene which is taken in different times. When this is the case, lower resolution image is resampled such that it has the same pixel size as the higher resolution one has. However, resampling does not improve the detail content of the lower resolution image, which is crucial for registration process. In change detection, generally, the lower resolution multispectral images are registered using the higher resolution ones for post-classification comparison. Registration needs common control points on both images. However, it is may be very difficult to select control point on poor resolution images. Thus, poor registration results in wrong land-cover change results. On the other hand, one object may contain area representative of more than one information class in the spatial domain. This can be regarded as spatial overlap (Tso and Mather, 2001), Spatial overlap of classes is the main difficulty in image classification to get high classification accuracies and reliable results from post-classification comparison. Another problem in pixel-based image classification is the mixed radiance values. Radiance value of an object is sensed by the sensor and assigned as the gray value of a particular pixel. However, the gray value of one particular object is affected by the neighboring objects due to atmospheric effects and the properties of the instrument optics. Hence, gray value of a pixel is affected by the gray value of the neighboring pixels (Tso and Mather, 2001).

In this study, the changes occurred on the costal zone of the city center of Trabzon due to a new major highway construction initiated along Black Sea cost in 2000 were evaluated. A 30 m resolution ETM+ multispectral image and a 4 m resolution IKONOS image acquired in 2000 and 2003, respectively, were only available multispectral image data in hand for post-classification comparison method (Figure 1). To tackle the poor spatial resolution problem and make major roads and other details smaller

than 30 m in size detectable, the ETM+ multispectral image was fused with its 15 m resolution panchromatic band using à trous image fusion algorithm. Thus, the post-classification comparison was performed between 4 m resolution IKONOS multispectral (4 m) and 15 m resolution fused ETM+ images.

MATERIALS AND METHODS

Pre-processing of the Input Images

The pre-processing of the input images is almost necessary for all change detection problems. This may include resampling, radiometric correction, histogram matching, possible registration and image fusion of the input images.

If possible, the remotely sensed data that have same spatial resolution is used for change detection process. However, it is still possible to perform change detection even if the spatial resolution of the input images does not match. In this case, lower resolution image is resampled such that it has the same pixel size as the higher resolution one has. Most image fusion algorithms also need resampling before fusion process since fusion essentially occurs when the involved images have the same spatial resolution. Thus, multispectral images may need to be resampled (generally up sampled) such that they have the same spatial resolution with the panchromatic image. The nearest neighbour method is the simplest one among resampling methods such as bilinear interpolation, bicubic approximation to sinc function, or 8-point or 10-point sinc function interpolation methods. In the nearest neighbour method, the new pixel value is assigned as the value of its nearest pixel. That is, the original pixel values repeat. However, other methods mentioned above interpolate new pixel values using the surrounding pixels, resulting in color content change in the original image Gungor and Shan, 2005). Therefore, nearest neighbour method is used for resampling to keep the original spectral properties of the multispectral image.

Ideally, the input images should have the same radiometric precision on both dates. In our case, ETM+ images have 8-bit precision, whereas IKONOS image has 11-bit resolution. When the radiometric resolution of data acquired by one system (8-bits) are compared with data acquired by a higher radiometric resolution instrument (11-bits), the lower resolution data should be decompressed to 11-bits for change detection purposes. In addition, to minimize the impacts of the atmospheric conditions, illumination and viewing angles, and soil moistures, images need to be radiometrically enhanced. For this purpose, histogram matching is applied between the input multispectral images. Matching the histogram of one image to that of another image makes the distribution of brightness values in the two images as close as possible. Thus, histogram matching is applied between original ETM+ and IKONOS multispectral images to make the histogram and the radiometric precision of the ETM+ resemble to those of IKONOS image as histogram matching also increases the radiometric precision of ETM+ image to 11-bits.

In some change detection algorithms such as post-classification comparison, it is essential to geometrically rectify the input images such that each pixel location on both input images represents the same location on the ground (Macleod and Congalton, 1998; Kwarteng and Chavez, 1998; Tardie and Congalton, 2004). This is done by registering the input images. Image fusion also requires geometric rectification of the input images since different images of the same area are used together. Registration can be done in various ways. The most accurate way is to register the input images separately by establishing geometric relationship between the

ETM+ Panchromatic
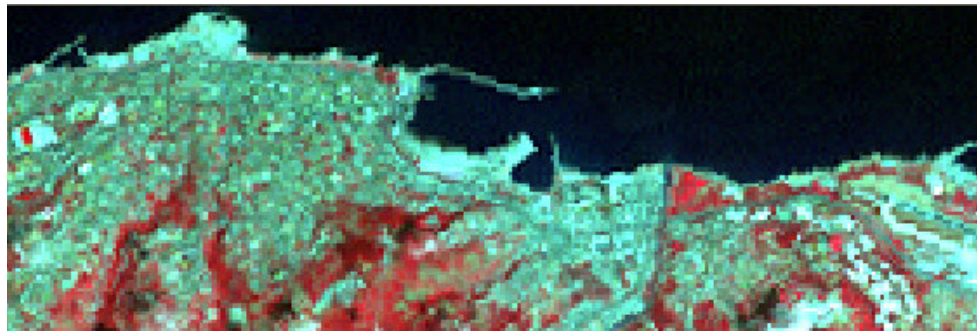
ETM+ Multispectral (Bands: 4,3,2)

IKONOS Multispectral (Bands: 4,3,2)

Figure 1. Remote sensing data used ETM+ panchromatic and multispectral image obtained in 2000 and IKONOS multispectral image obtained in 2003.

image and the ground using rigorous photogrammetric methods (Lee and Bethel, 2001). This process is called georegistration. The georegistration process can also be done for pushbroom imaging systems such as IKONOS and Quickbird sensors (Lee and Bethel, 2001). Another way of registering the input images is to use polynomial transforms. When ground control is known, such transform can be performed to the ground truth, otherwise it can be applied between images. In this case, one image (generally, the one that have better resolution) is taken as the reference and the other one is registered using this reference image. The accuracy of image registration is usually conveyed in terms of root-mean-square (RMS) error. In this study, the first order polynomial transformation method is used for registration refinement of multispectral images by taking the IKONOS multispectral image as the reference. Common points on both images are selected carefully such that they produce an RMS error smaller than 0.5 pixels with respect to the pixel size of the fused ETM+ image.

Image fusion methods are designed to increase the spatial resolution of the multispectral images without distorting their spectral contents. The missing spatial detail in the multispectral images are found and then transferred into the multispectral images with the help of higher spatial resolution panchromatic one. Hence, higher resolution images highlight linear features on the images, such as roads, build up areas and coastlines, which leads to better registration of the input images and more accurate post-classification comparison results. Image fusion algorithms are categorized as color-based, wavelet transform-based and statistical methods (Gungor, 2008). Examples of color-based fusion include IHS (Intensity, Hue, and Saturation), Brovey, and SVR (Synthetic Variable Ratio) methods. Mallat's multiresolution, the à trous, and M-Band wavelet transform approaches are the most common wavelet transform-based fusion algorithms, and statistical image fusion methods include Principal Component Analysis (PCA), linear regression method (Price, 1999), spatially adaptive image fusion (Park and Kang, 2004), σ - μ method (Gungor and Shan, 2005), and criteria-based method (Gungor, 2008). The wavelet transform-based fusion methods are successful in terms of keeping the color quality of the original multispectral images; however, their
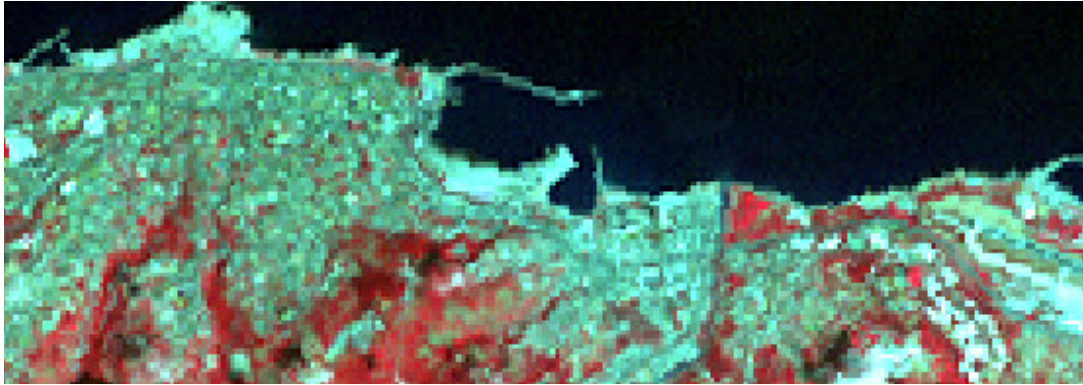
ETM+ Multispectral (Bands: 4,3,2)
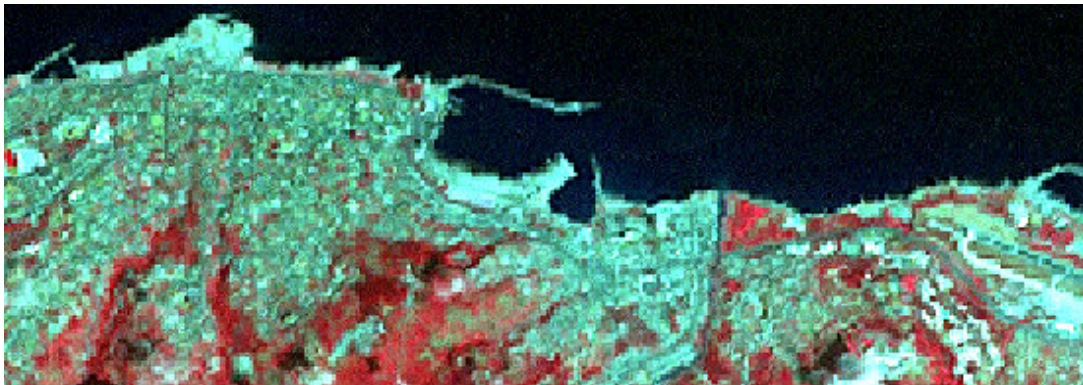
Fused ETM+ Multispectral (Bands: 4,3,2)

Figure 2. Fusion of ETM+ multispectral and panchromatic bands.

performances are not appealing as the results obtained from color-based and statistical methods in terms of improving the spatial detail content (Gungor, 2008). On the other hand, color-based and statistical methods are not successful as the wavelet-transform based methods in terms of color quality. This study uses multispectral images for image classification to detect the changes occurred in the scene. Therefore, keeping the color quality of the original multispectral image is crucial. For this reason, the à trous wavelet transform method, one of the most successful representative of the wavelet-transform based fusion methods, is chosen as the fusion method since it is fast and easy to implement, and reliable in terms of good color quality. The spatial resolution of ETM+ multispectral data is improved from 30 - 15 m using 15 m spatial resolution panchromatic image via à trous image fusion algorithm. Then, 4 m resolution IKONOS multispectral image and 15 m resolution fused ETM+ multispectral image is registered and used for classification. The original and fused ETM+ images are displayed in Figure 2.

The à trous algorithm is a non-orthogonal, dyadic, undecimated, DWT algorithm. It uses a low-pass filter associated to a scale function $\phi(t)$ to obtain successive approximations of the original image. It also uses a high-pass filter to get three detail images (Aiazzi et al., 2002). Instead of decimation during the transform, the low-pass and high-pass filters are up-sampled by inserting $2^{j-1}-1$ zeros between the filter coefficients at each decomposition level j to reduce the resolution of the original image (Wegner et al., 2006). Since decimation is not applied, approximation and detail images have the same size as the original input images at every decomposition level. The inverse transform gets the original image

by using two synthesis filters.

There is also a practical implementation of the à trous wavelet transform algorithm (Starck and Murtagh, 1994). This algorithm uses a scaling function, a B-spline of degree 3, which leads to the following 2-D 5x5 convolution mask H_0.

$$H_0 = \frac{1}{256} \begin{bmatrix} 1 & 4 & 6 & 4 & 1 \\ 4 & 16 & 24 & 16 & 4 \\ 6 & 24 & 36 & 24 & 6 \\ 4 & 16 & 24 & 16 & 4 \\ 1 & 4 & 6 & 4 & 1 \end{bmatrix}$$

To calculate the approximation image that contains the high frequency part of the original image, the low-pass filter is up-sampled before each decomposition level by inserting zeros between filter coefficients using the same methodology explained above. The detail image w, which contains the high frequency part of the original image, is obtained as the difference of two successive approximation images. For image fusion, each multispectral band I_k^M, where k denotes the k-th multispectral band, is resampled to the same size of the panchromatic image I_0^P. Then, I_0^P is decomposed until the resolution of I_j^P (in terms of spatial detail content, not pixel size) equals to the resolution of I_k^M. Next, summation of $\{w_j\}$ is calculated as
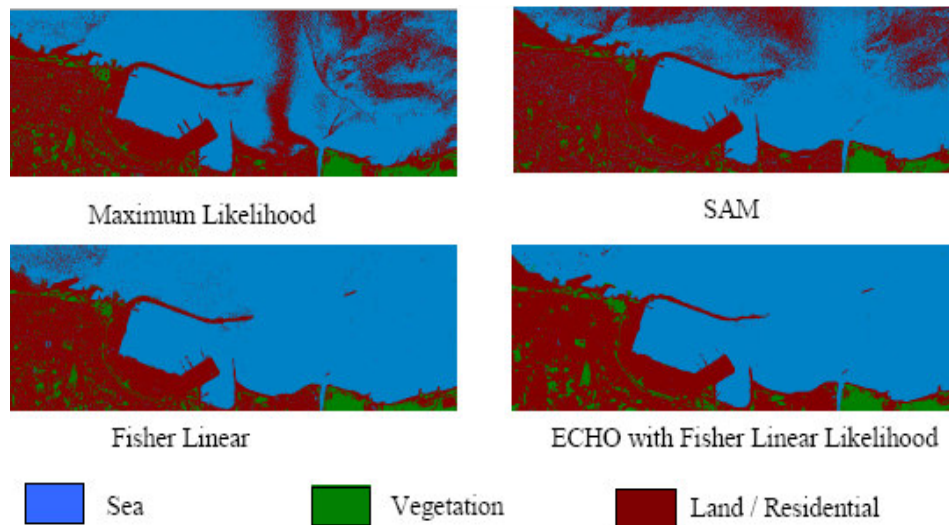
Figure 3. Classification results of IKONOS multispectral image using ML, SAM, FLL, and ECHO with fisher linear likelihood algorithms

$W = \sum_{j=1}^{J} w_j$ to detect the spatial detail difference between panchromatic and multispectral image. Finally, W is added to each original multispectral band I_k^M to construct *k-th* fused band. The number of decomposition level is determined with respect to the resolutions of the panchromatic and the multispectral images. For example, for ETM+ panchromatic and multispectral images case, one level wavelet decomposition to the panchromatic image is enough to make its resolution the same as the multispectral image since the resolution of the multispectral image is two times coarser than the panchromatic image.

Post-classification comparison

Once input images are pre-processed for change detection, next step is to decide on a change detection algorithm. In the literature, many change detection algorithms are available. Tardie and Congalton (2004) use multi-date visual composite, image differencing, and post-classification algorithms are used for change detection problems (Tardie and Congalton, 2004). Furthermore, cross-correlation analysis, multi-date principal components analysis and RGB-NDVI color composite change detection is added to these methods (Civco et al., 2002). Additionally, techniques such as spectral mixture analysis, the Li–Strahler canopy model, Chi-square transformation, fuzzy sets, artificial neural networks and integration of multi-source data that have been used for change detection applications.

In this study, post-classification comparison method is adopted as standard change detection algorithm. In this technique, two images from different dates are separately classified. Then, classified images are compared pixel by pixel to create a new change image, which indicates the changes that took place as "from" and "to" information (Tardie and Congalton, 2004; Mas, 1999). Since input images are classified separately, atmospheric effects, sensor and environmental differences between multi-temporal images are minimized and a complete matrix of change information is obtained (Lu et al., 2004).

Accurate classification is very important for reliable change detection results as the final accuracy depends on the quality of the classified image of each date (Lu et al., 2004). Therefore, choosing the best classification algorithm, depending on the nature of the data, is crucial. IKONOS image was taken in 2003 after a heavy rain in Black Sea Region; therefore, the surface of the Black Sea was rough because of waves resulting from windy weather. Degirmendere Creek that flows into the Black Sea was also carrying mud and sediments as a result of heavy rain and caused intensive color change in water especially at the river mouth and its vicinity. Accordingly, wave patterns and sediments at the river mouth could provoke misclassification of pixels as land in Black Sea, and misclassification affects the post classification comparison results negatively. Thus, input images are classified using Maximum Likelihood (ML), SAM (Spectral Angular Mapping), Fisher Linear Likelihood (FLL), and ECHO classifiers and best result is obtained from ECHO classifier. ECHO is a spatial-spectral classifier that incorporates not only spectral variations but spatial ones as well as into the decision-making process. It is a classifier that first segments the scene into spectrally homogenous objects. Then, it performs a sample classification algorithm based upon a maximum likelihood object classification scheme in which each object delineated would be classified based on the statistical properties of the pixels of the object (Landgrebe, 2003).

RESULTS AND DISCUSSION

Preliminary classifications were performed on the fused ETM+ and IKONOS multispectral images to carry out a post-classification analysis procedure. Classification of both images are performed using Maximum Likelihood (ML), SAM (Spectral Angular Mapping), Fisher Linear Likelihood (FLL), and ECHO with FLL classifiers. Results show that, ML, SAM, and FLL classifiers misclassify the wave patterns and sediments carried to the Black Sea through Degirmendere Creek, particularly in IKONOS image (Figure 3). The best classification result was obtained using ECHO classifier with fisher linear algorithm by combining the spectral information with

Table 1. Training class performance (resubstitution method) for IKONOS image.

Class name	Reference accuracy (%)	# of samples	Number of samples in class									
			Sea	River	Grass	Road	Shadow	Trees	Bld_Type 1	Bld_Type 2	Bld_Type 3	Bare Soil
Sea	96.7	23319	22561	15	0	1	733	0	6	3	0	0
River	100.0	2754	0	2754	0	0	0	0	0	0	0	0
Grass	89.1	7309	0	0	6511	0	0	798	0	0	0	0
Road	99.7	5825	0	3	0	5810	0	0	0	4	7	1
Shadow	99.0	777	8	0	0	0	769	0	0	0	0	0
Trees	87.1	3366	1	0	3	0	93	3269	0	0	0	0
Bld _Type1	97.7	259	4	0	0	0	0	0	253	0	0	2
Bld_Type2	96.4	111	0	0	0	4	0	0	0	107	0	0
Bld_Type3	25.0	326	0	13	0	227	0	0	0	2	84	0
Bare Soil	100.0	287	0	0	0	0	0	0	0	0	0	287
Total		44333	22574	2785	6514	6042	1595	4067	259	116	91	290
Reliability Accuracy (%)			99.9	98.9	100.0	96.2	48.2	80.4	97.7	92.2	92.3	99.0

Overall Class Performance (42405 / 44333) = 95.7%.
Kappa Statistic (X100) = 93.6%. Kappa Variance = 0.000002.

Table 2. Training class performance (resubstitution method) for ETM+ image.

Class name	Reference accuracy (%)	# of samples	Number of samples in class								
			Sea	River	Grass	Trees	Bld_Type 1	Road	Shadow	Bld_Type 2	Bld_Type 3
Sea	71.3	34738	24756	9982	0	0	0	0	0	0	0
River	72.2	5834	1396	4211	0	7	0	117	103	0	0
Grass	90.0	20862	0	0	18778	1901	0	126	8	0	49
Trees	100.0	960	0	0	0	960	0	0	0	0	0
Bld_Type1	88.1	2141	0	0	0	0	1886	171	0	0	84
Road	80.8	8934	47	294	0	0	297	7219	944	35	98
Shadow	74.5	635	74	88	0	0	0	0	473	0	0
Bld_Type2	91.5	364	0	0	0	0	0	31	0	333	0
Bld_Type3	97.9	96	0	0	0	0	0	2	0	0	94
Total		74564	26273	14575	18778	2868	2183	7666	1528	368	325
Reliability Accuracy (%)			94.2	28.9	100.0	33.5	86.4	94.2	31.0	90.5	28.9

Overall Class Performance (58710 / 74564) = 78.7%.
Kappa Statistic (X100) = 71.1%. Kappa Variance = 0.000004.

spatial information. The misclassified pixels on Black Sea are eliminated substantially with ECHO classifier.

In IKONOS image, 10 classes (Sea, River, Grass, Road, Shadow, Trees, Building_Type1, Building_Type2, Building_Type3, and Bare Soil) were determined to classify the scene. Analogously, the same procedure is performed for the fused ETM+ image; however, 9 classes were selected by omitting the class Bare Soil since it was not possible to select this class on ETM+ image due to its relatively course resolution. Training class performances

for both images are given in Table 1 and Table 2. Overall class performances for IKONOS and fused ETM+ images are 95.7 - 78.7% and Kappa statistics are 93.6 - 71.1%, respectively. These figures indicate that the classification accuracy of the fused ETM+ image is lower than the one obtained from the IKONOS image. Since the classes could be selected more precisely in IKONOS image, it has a better classification performance both visually and quantitatively. After classification, all classes are grouped as three final classes as sea, vegetation, and

Classification Results of ETM+ Image

Classification Results of IKONOS Image
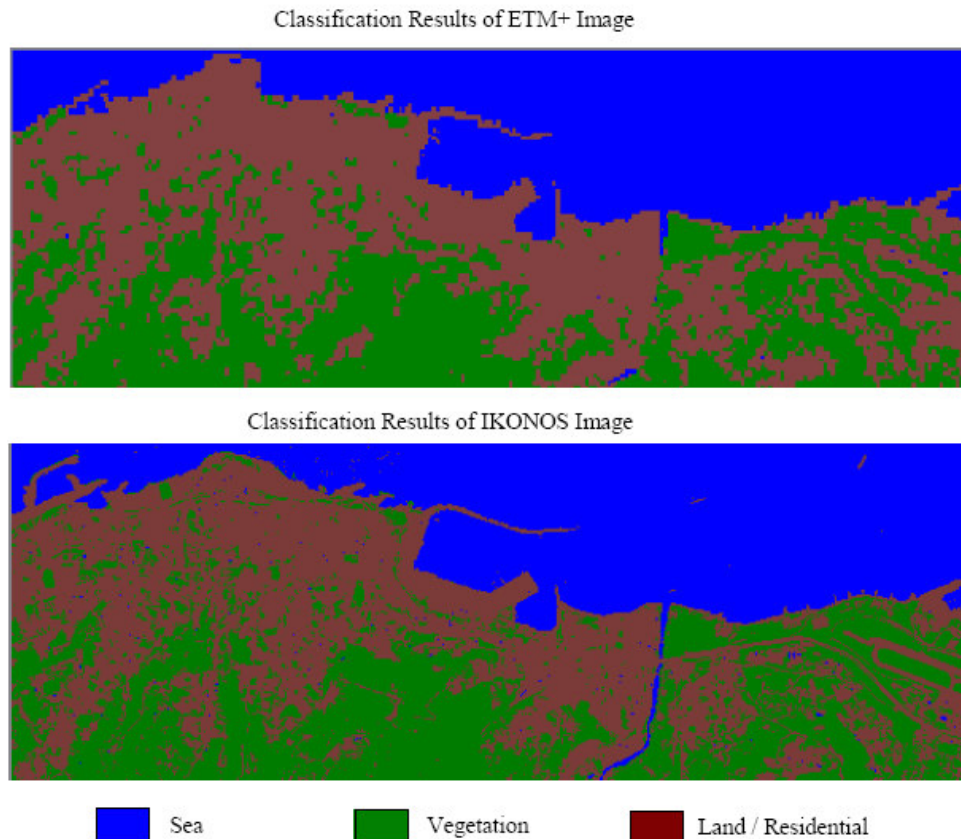
Figure 4. Preliminary classification results for ETM+ and IKONOS images.
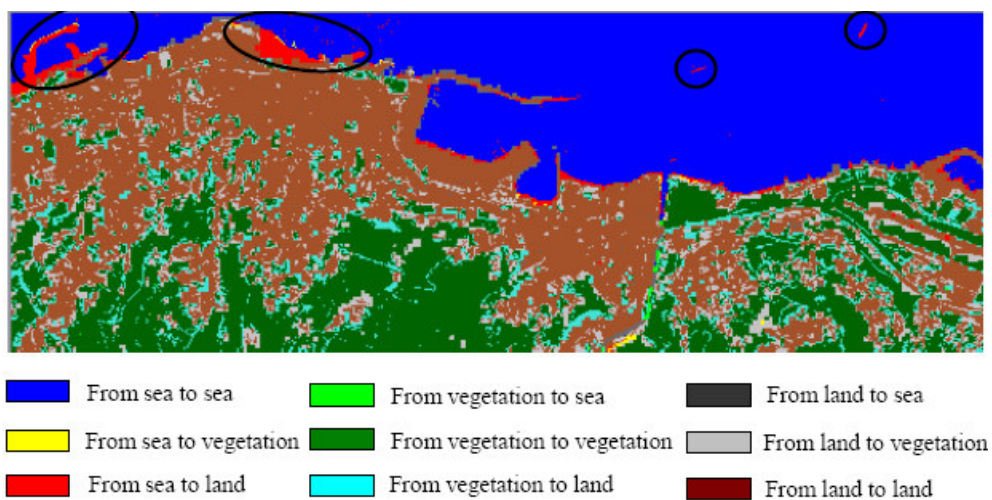
Figure 5. Change image showing the differences between 2000 and 2003.

Land/Residential. Sea and River was grouped as Sea, Grass and Trees are grouped as Vegetation, and Land, Shadow, Building_Type1, Building_Type2, and Building_ Type3 were grouped as Land/Residential. Classification results are displayed in Figure 4. Then, both classified images were recoded and used for post-classification comparison procedure in ERDAS IMAGINE software. As the output, the change image and the confusion matrix which contains the "from" and "to" information were generated. The change image is illustrated in Figure 5, and the confusion matrix is given in Table 3.

Table 3 displays both thematic and quantitative

Table 3. Confusion matrix.

		ETM+ (2000)		
		Sea (ha)	Vegetation (ha)	Land / Residential (ha)
	Sea (ha)	517.89	1.24	12.90
IKONOS (2003)	Vegetation (ha)	2.00	359.48	121.58
	Land / Residential (ha)	23.23	95.15	525.42

information about changes. The colors used in Table 3 are the the same as the ones used in Figure 5 to illustrate "from" and "to" information of different classes. If the pixels classified as Sea in fused ETM+ image did not change in IKONOS image, these pixels are displayed in blue in Figure 5 and the total area covered by these pixels are computed as 517.89 ha. Similarly, if the pixels classified as Land / Residential in the fused ETM+ image classified as Vegetation in IKONOS image, these pixels are displayed in light gray in Figure 5 and the total area covered by these pixels are calculated as 121.58 ha. Total area for each change is found by multiplying the number of changed pixels with 16 square meter (area of one pixel on both images), and then, converting to hectares. Hence, elaborating Table 3 reveals that an area of 23.23 ha turned into land from sea. This area is displayed in red in Figure 5 and showed with in ellipses. The red objects in Black Sea, which are showed in two circles, are ships approaching to the port. These ships were classified as land in IKONOS image and detected as change (from Sea to Land/Residential) after post classification comparison. When Figure 4 is visually inspected, it can be concluded that pattern in Vegetation and Land/Residential classes do not have a significant change between 2000 - 2003. However, Table 3 shows that there are considerable "from" and "to" changes between these classes. The reason of this change lies in the spatial resolution difference of both images. Even though spatial resolution of the original ETM+ was enhanced and made 15 m, still there is a large difference between 4 m resolution IKONOS image. The vegetation between buildings and on refuges and traffic islands are distinguishable from the other classes on IKONOS image and classified correctly. However, the same area on the fused ETM+ image could not classified correctly due to its low resolution. Therefore, an area of 121.58 ha is detected as change from Vegetation in the fused ETM+ to Land/Residential in IKONOS image. This result implies that the performance of the change detection process may be worse, if image fusion had not been applied to the original ETM+ image.

Conclusion

In this study, the change on costal zone of Trabzon is detected using two satellites images having different spatial resolutions. As expected, the land fill on costal zone due to new high way construction is detected successfully. It is seen from the visual inspection of individual classification results that the land-cover and land-use in Trabzon does not have a pattern of change. The changes in these classes detected in post-classification results are mainly due to the relatively poor spatial resolution of the fused ETM+ image. Improving the spatial resolution of the ETM+ using à trous wavelet transform algorithm minimizes the impact of misclassification on final change image generated by post-classification comparison.

Classifiers such as maximum likelihood and fisher linear likelihood misclassify wave patterns in IKONOS image as bare soil. This problem is misinterpreted by post-classification comparison and perceived as a change from sea to Land/Residential class. This problem is fixed using ECHO classifier, which combines the spectral information with spatial information.

REFERENCES

Aiazzi B, Alparone L, Baronti S, Garzelli A (2002). Context-Driven Fusion of High Spatial and Spectral Resolution Images Based on Oversampled Multiresolution Analysis. IEEE Trans. on Geoscience and Remote Sensing 40(10): 2300-2312.

Chen LC, Rau JY (1998). Detection of shoreline changes for tideland areas using multi-temporal satellite images. Int. J. Remote Sensing. 19(17): 3383-3397.

Civco DL, Hurd JD, Wilson EH, Song M, Zhang Z (2002). A Comparison of Land Use and Land Cover Change Detection Methods. ASPRS-ACSM Annual Conference and FIG XXII Congress.

Gungor O (2008). Multi Sensor Multi Resolution Image Fusion. PhD Dissertation, Purdue University, Indiana, USA.

Gungor O, Shan J (2005). A statistical approach for multi-resolution image fusion. UPPECORA 16UP - "Global Priorities in Land Remote Sensing", held at Sioux Falls Convention Center, Sioux Falls, SD, USA.

Huang W, Fu B (2002). Remote Sensing for Coastal Area Management in China. Coastal Management 30: 271-276.

Kwarteng AY, Chavez PS (1998). Change detection study of Kuwait City and environs using multitemporal Landsat Thematic Mapper data. Int. J. Remote Sensing 19(9): 1651-1662.

Landgrebe DA (2003). Signal Theory Methods in Multispectral Remote Sensing, John Wiley&Sons, Hoboken, New Jersey, USA.

Lee C, Bethel J (2001). Georegistration of Airborne Hyperspectral Image Data. IEEE Trans. on Geoscience and Remote Sensing. 39(7): 1347-1351.

Lu D, Mausel P, Brondizio E, Moran E (2004). Change detection techniques. Int. J. Remote Sens. 25(12): 2365-2407.

Macleod RD, Congalton RG (1998). A Quantitative Comparison of Change-Detection Algorithms for Monitoring Eelgrass from Remotely Sensed Data. Photogrammetric Eng. Remote Sens. 64(3): 207-216.

Mas JF (1999). Monitoring land-cover changes: a comparison of change detection techniques. Int. J. Remote Sens. 20(1): 139-152.

Park JH, Kang MG (2004). Spatially adaptive multi-resolution multispectral image fusion. Int. J. Remote Sens. 25(23): 5491-5508.

Price JC (1999). Combining Multispectral Data of Differing Spatial Resolution. IEEE Trans. Geosci. Remote Sens. 37(3): 1199-1203.

Ramachandra TV, Kumar U (2004). Geographic Resources Decision Support System for land use, land cover dynamics analysis. Proceedings of the FOSS/GRASS Users Conference held in Bangkok, Thailand.

Starck JL, Murtagh F (2004). Image Restoration with Noise Suppression Using the Wavelet Transform. Astron. Astrophys. 288: 342-348.

Tso B, Mather PM (2001). Classification Methods for Remotely Sensed Data, Taylor and Francis. London and New York.

Wegner FV, Both M, Fink RHA (2006). Automated Detection of Elementary Calcium Release Events Using the A Trous Wavelet Transform. Biophys. J. 90: 2151-2163.